Journal of Materials Science: Materials in Electronics (2018) 29:12871–12877
https://doi.org/10.1007/s10854-018-9406-4

Core–shell $NiCo_2O_4$@$ZnWO_4$ nanosheets arrays electrode material deposited at carbon-cloth for flexible electrochemical supercapacitors

Kaihua Zhang[1] · Liyang Lin[1] · Shahid Hussain[2] · Song Han[1]

Received: 26 March 2018 / Accepted: 1 June 2018 / Published online: 5 June 2018

Abstract
Three dimensional (3D) hierarchical $NiCo_2O_4$ nanosheet arrays (NSAs)@$ZnWO_4$ nanoflakes (NFs) core–shell structures have been successfully grown on a carbon cloth (CC) using two-step hydrothermal approach, following a heat treatment route. Compared with the pure CC@$NiCo_2O_4$ NSAs electrode, the binder-free CC@$NiCo_2O_4$@$ZnWO_4$ hybrid system gives rise to a higher specific capacitance of 872.0 Fg^{-1} at a low current density of 1 Ag^{-1} and 791.1 Fg^{-1} at a quite high current density of 20 Ag^{-1}, and retains ~ 92.9% of the initial capacitance even after 5000 cycles of charge and discharge. The excellent electrochemical performance of CC@$NiCo_2O_4$@$ZnWO_4$ electrode is attributed to its high specific surface area of the 3D structures, fast electron transport property of $NiCo_2O_4$ material as the skeleton, and the synergistic effect between $NiCo_2O_4$ and $ZnWO_4$ materials, demonstrating that CC supported $NiCo_2O_4$ NSAs@$ZnWO_4$ NFs composite as the high-performance electrode materials are highly desirable for the application of flexible supercapacitors.

1 Introduction

Fast developing stretchable devices, collapsible displays, and wearable electronics significantly booms the demand of suitable flexible energy powering sources [1]. Supercapacitors have attracted considerable attention in the field of energy storage due to their high power density, fast charge–discharge (CD) rate, and ultra-long cycle lifetime [2–5]. In recent years, some metal substrates have been wildly used as the current collectors or electrically conductive substrates to grow metal oxides/hydroxides on the surface directly without any binders, which can improve the electrical conductivity of the whole system [6–10]. However, these metal substrates not only contribute little capacitance to the supercapacitor devices by themselves, but also cannot bear the mechanical distortion without break.

In order to meet the requirement of flexible supercapacitor devices, many carbon based three dimensional substrate have been designed and used in the electrochemical fields [11–15]. The cheap but flexible/bendable carbon cloth (CC) has already attracted extensive research for a generation of electronic devices in various applications [16–19]. Unfortunately, because of the limited surface area, it is difficult to grow complex metal oxides nanostructures on the surface of CC, which results in the serious shortage of the effective electrode materials. A novel and skillful strategy is constructing the electrode composite materials with 3D core–shell structures on the skeleton of CC. Such hierarchical 3D synergistic nanostructures can provide a quite large surface area to facilitate easy access of electrolyte ions into the whole system [20–23]. Moreover, the synergistic effect between two different electrode materials can enhance the electrochemical performance, for instance, the promotion of the specific capacitance and the cycle performance [24–26]. Almost all of the systems containing two electrode materials have been reported, but there is a promising electrode material $ZnWO_4$ is rarely reported as the composite materials for supercapacitors [27]. In addition, $NiCo_2O_4$ as a common electrode material has been widely reported owing to its outstanding electrical conductivity and high redox activity, which are very favorable and suitable for the "core" part in the core–shell system [28–31]. It is expected that advancements in anode electrodes can be achieved by combining the flexible CC and hierarchical 3D $NiCo_2O_4$@

✉ Liyang Lin
jack_linliyang@cqu.edu.cn

✉ Shahid Hussain
shahid@ujs.edu.cn

[1] College of Aerospace Engineering, Chongqing University, Chongqing 400044, China

[2] School of Materials Science and Engineering, Jiangsu University, Jiangsu 212013, China

$ZnWO_4$ core–shell structures in a complete supercapacitor configurations.

Herein, we reported a synthesis of 3D $NiCo_2O_4$ NSAs@ $ZnWO_4$ NFs core–shell structures grown on CC by a facile and efficient two-step hydrothermal method. This special system as both a new class of binder-free anode and the current collector instead of traditional 2D or 3D metal current collectors such as copper, titanium plates and Ni foam, exhibiting high specific capacitance, good rate capability, and great cycle performance. The CC@$NiCo_2O_4$@$ZnWO_4$ electrode possessed a high specific capacitance of 872.0 Fg^{-1} at a current density of 1 Ag^{-1}, 791.1 Fg^{-1} at a high current density of 20 Ag^{-1}, and still retained 92.9% capacitance even after 5000 cycles.

2 Experimental

2.1 Materials preparation and characterization

All the regents that were used in the experiment are analytical grade without any further purification. Firstly, a piece of CC (2 cm × 3 cm) was adequately washed to remove the dirty by continuous ultrasonication in acetone, ethanol, and deionized (DI) water for 15 min, respectively.

To grow $NiCo_2O_4$ NSAs on the CC (S_1), 2 mmol cobalt nitrate hexahydrate, 1 mmol nickel nitrate hexahydrate, 1 g cetyltrimethyl ammonium bromide (CTAB) were dissolved in 40 mL mixed solution (34 mL methyl alcohol and 6 mL DI water) under magnetic stirring for 30 min. The solution was subsequently transferred into a 50 mL Teflon-lined stainless steel autoclave. A piece of treated CC (2 cm × 3 cm) was immersed in the solution before sealing the autoclave. Then, the autoclave was put into an electric oven and heated at 180 °C for 12 h. The precursors grown on the CC were rinsed several times with ethanol and DI water. Finally, S_1 was obtained after annealing in the muffle furnace at 350 °C for 2 h.

To fabricate CC@$NiCo_2O_4$@$ZnWO_4$ NSAs core–shell structures (S2), 1 mmol zinc nitrate hexahydrate, 1 mmol sodium tungstate, and 6 mmol ammonium fluoride were dissolved in 40 mL DI water under magnetic stirring for 30 min. Then, the milky suspension was transferred into a 50 mL Teflon-lined stainless steel autoclave with as-obtained S_1. The autoclaves was put into the electric oven and heated at 180 °C for 6 h. The final products were washed with DI water and dried at 60 °C for 6 h following a heat treatment in the muffle furnace at 400 °C for 2 h to obtain S_2.

The composition and phase of the samples were evaluated by X-ray diffraction (XRD). Morphologies, elemental map and nanostructures were characterized with a JSM-7800F (JEOL) field-emission scanning electron microscope (FE-SEM) and a JEM-2100F (JEOL) Transmission Electron Microscope (TEM).

2.2 Electrochemical measurements

A common three-electrode system was used for the test of electrochemical performance. The electrodes made of S_1 and S_2 were used as working electrodes. Saturated calomel electrodes and Pt foil was used as reference and counter electrodes, respectively. Cyclic voltammetry (CV) and galvanostatic charge–discharge (GCD) measurements were conducted in 2.0 M KOH solution by an electrochemical working station. The specific capacitance (C) was calculated by using $C = I\Delta t/m\Delta U$ in the discharge measurements, where I is discharge current density, ΔU is the width of the potential window, m is the mass of the active materials and Δt is the discharging time [32, 33]. The effective region of the electrodes immersed in the electrolyte was controlled to be ~ 1 × 1 cm^2. The mass loading of the S_1 and S_2 electrodes for the three-electrode system was ~ 0.82 mg and ~ 1.2 $mgcm^{-2}$, respectively.

3 Results and discussion

3.1 Structural characterization and analysis

A simple schematic illustration of formation process of CC@$NiCo_2O_4$ NSAs@ $ZnWO_4$ NFs core–shell structures are shown in Fig. 1. The corresponding X-ray diffraction (XRD) patterns of the CC@$NiCo_2O_4$@$ZnWO_4$ sample that was tested as the thin-film materials are presented in Fig. 2, including the standard patterns of $NiCo_2O_4$ (JCPDS 20–0781) and $ZnWO_4$ (JCPDS 15–0774). Obviously, it contains three different phases. Four diffraction peaks at 36.8°, 44.7°, 59.3° and 65.0° correspond to (311), (400), (511) and (440) planes of $NiCo_2O_4$. A peak appearing at 26.4° corresponds to (002) plane of C (JCPDS 41-1487). Other peaks at 23.8°, 24.6°, 30.5°, 36.4°, and 53.6° correspond to (011), (110), (111), (002) and (-202) plane can be identified as $ZnWO_4$. It can be confirmed that as-prepared product is with no impurities.

Surface morphologies of S_1 and S_2 have been observed and recorded by SEM shown in Fig. 3. In detail, Fig. 3a, b, d, e show the low-magnification SEM images of S_1 and S_2 revealing that almost all the carbon fibers are covered by $NiCo_2O_4$ or $NiCo_2O_4$@$ZnWO_4$ composite even after a comprehensive rinsing by DI water and ethanol. From the high-magnification SEM image (Fig. 3c) of S_1, one can notice that these well-ordered $NiCo_2O_4$ nanosheets (length of 1 ~ 2 μm) are grown vertically and cross-linked on the carbon fiber. For the feature of S_2, Fig. 3f indicates that each piece is fully decorated by a number of small and dense flakes (length

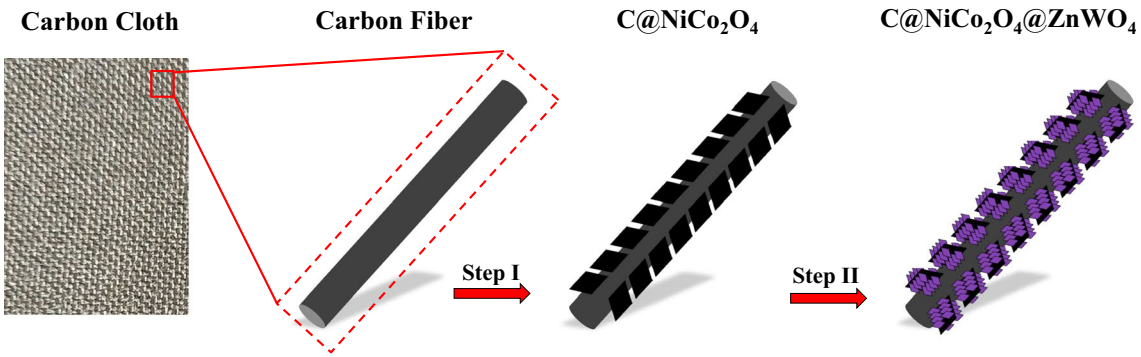

Fig. 1 Steps wise schematic diagram for the formation of nanostructures deposited on carbon cloth

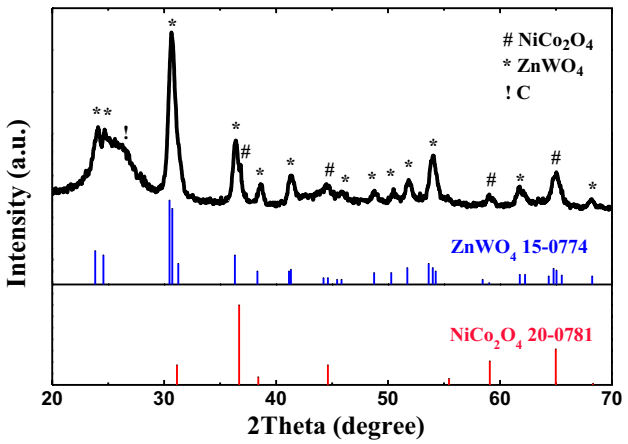

Fig. 2 XRD patterns of CC@$NiCo_2O_4$@$ZnWO_4$ NSAs core–shell structures

of 150 ~ 200 nm). Furthermore, the EDS mappings including W, Zn, Ni, Co, and O are also displayed separately in Fig. 4, roughly confirming the uniformly distribution of these elements.

To probe nanostructures of both S_1 and S_2, we conducted TEM and HRTEM imaging of a single $NiCo_2O_4$ NS and $NiCo_2O_4$@$ZnWO_4$ core–shell NS scraped from the CC respectively, as shown in Fig. 5. Figure 5a illustrates that the $NiCo_2O_4$ nanosheet is flat but with many pores (a lot of white plots) on the surface according to the whole contrast, which should be attributed to the thermal-dynamical decomposition from the precursor $Ni_xCo_{2x}(OH)_{6x}$ to final product [34]. In addition, Fig. 5b as the HRTEM image of S_1 shows one set of lattice fringes from $NiCo_2O_4$ nanosheet (the width of 0.245 nm) corresponds to (311) crystal plane of $NiCo_2O_4$ phase. From Fig. 5c, the core–shell structures

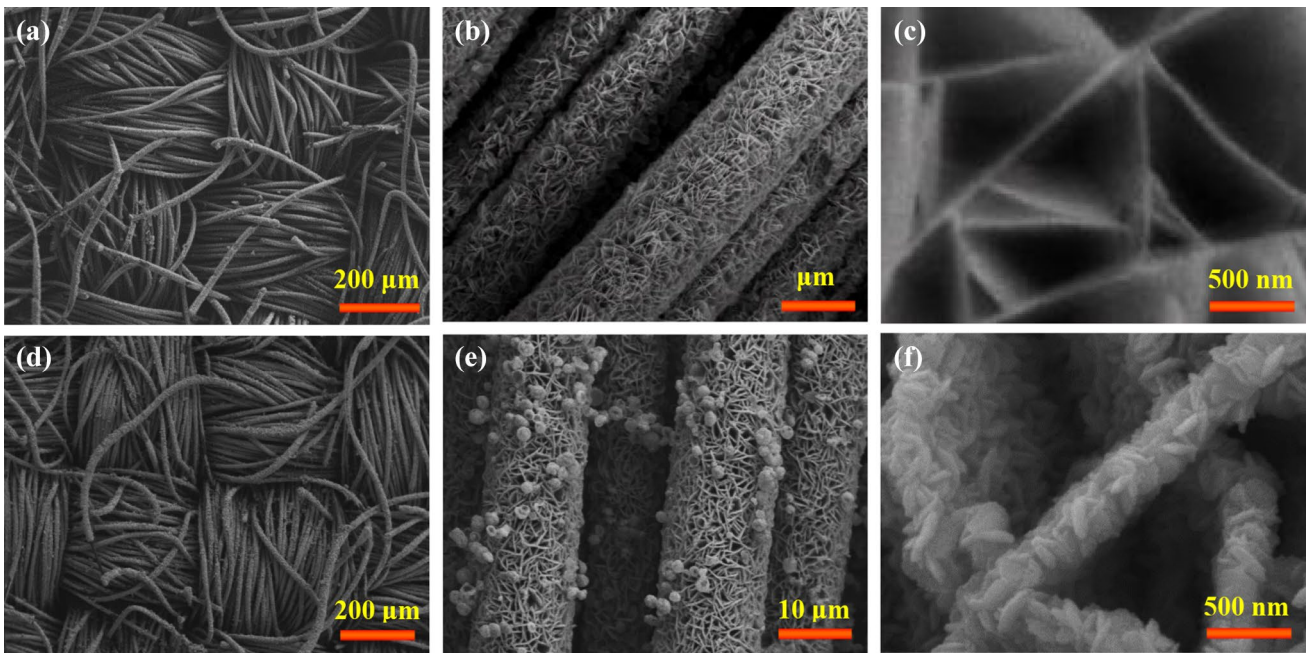

Fig. 3 SEM images of **a**–**c** S_1 and **d**–**f** S_2

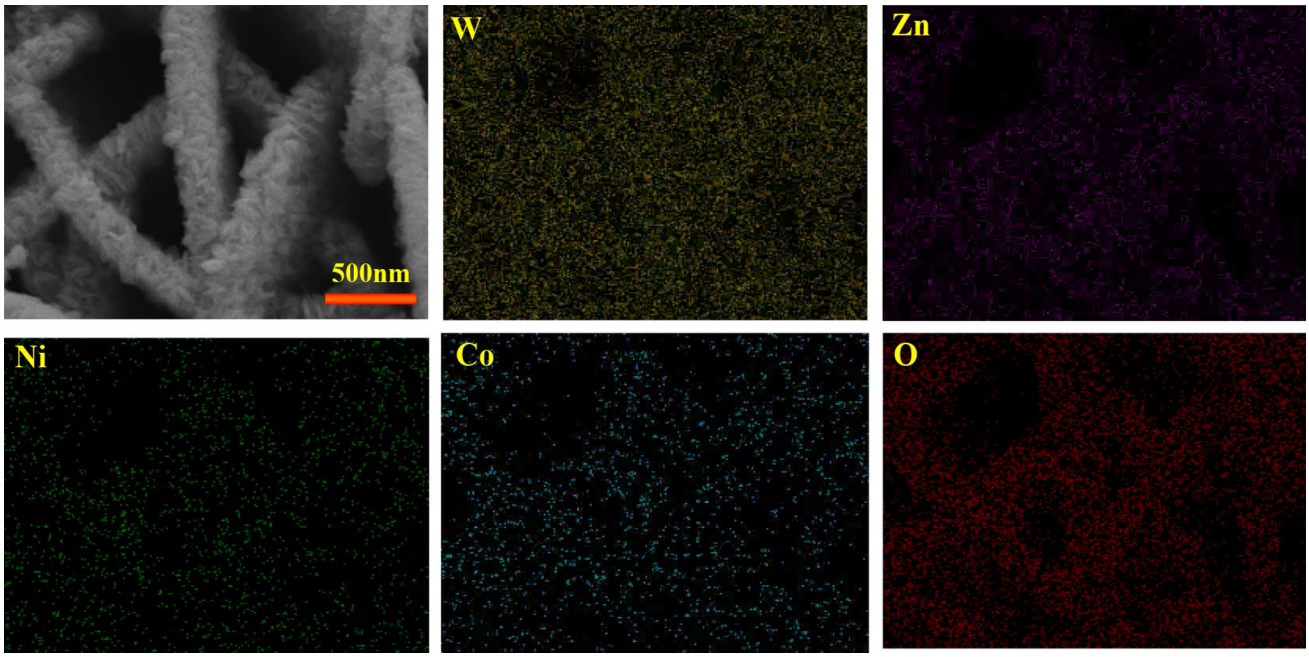

Fig. 4 SEM image and EDS mappings of S_2

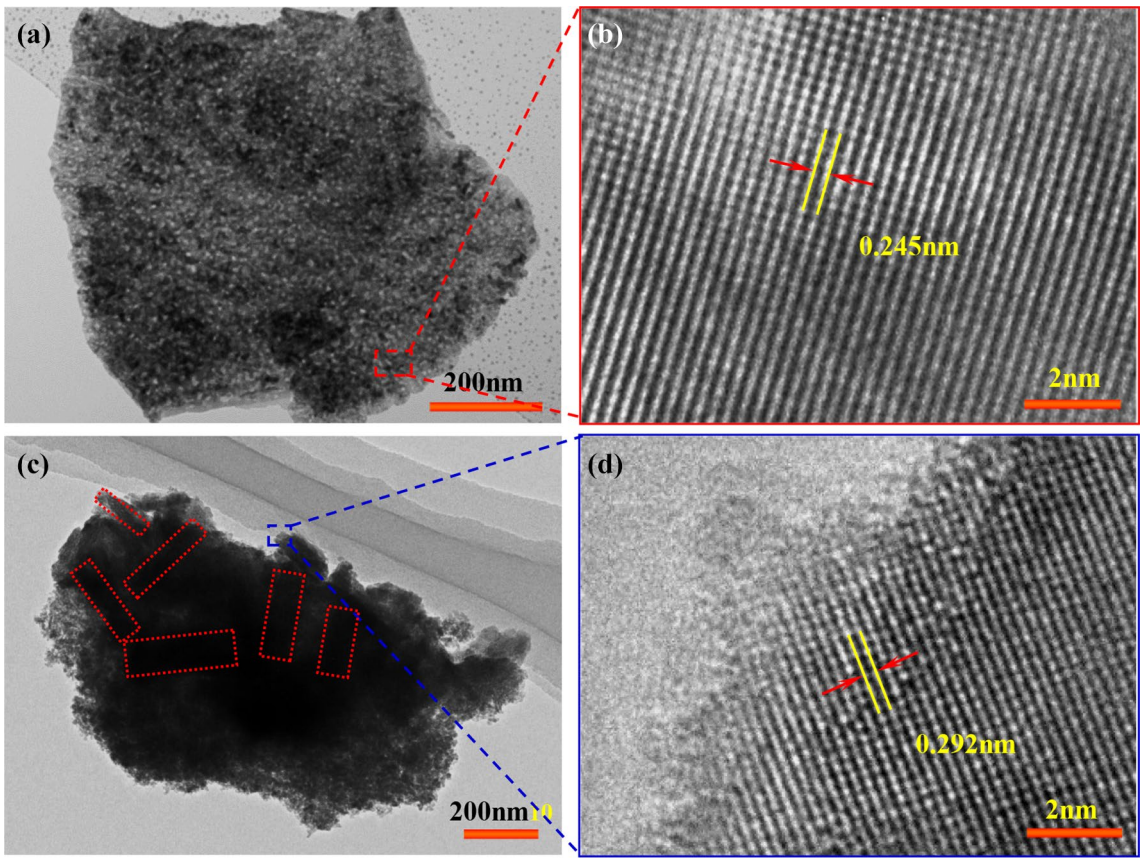

Fig. 5 TEM and HRTEM images of **a, b** S_1 and **c, d** S_2. (Color figure online)

can be observed based on the different contrast comparing with Fig. 5a. Clearly, the flat flake facing us with a larger size should be $NiCo_2O_4$ nanosheet. Some black lines (marked with red dotted lines) are about width of 150 nm, which matches the characterization of SEM image Fig. 3f, corresponding to the small-size vertical $ZnWO_4$ NFs. The HRTEM image (Fig. 5d) that obtained from one end of a black line shows one set of lattice fringes (the width of 0.292 nm) corresponds to (111) crystal plane of $ZnWO_4$ phase.

3.2 Electrochemical characterization and analysis

To test their potential application as supercapacitors, we studied electrochemical performance of both electrodes S_1 and S_2. Figure 6a shows the cyclic voltammetry (CV) curves with the potential window ranging from 0 to 0.7 V at a sweep rate of 100 mVs^{-1} for the electrode S_1 and S_2, respectively. As expected, the region surrounded by the CV curve for the electrode S_2 is broader than that for the electrode S_1. Moreover, the positions of redox peaks are also different. For the electrode S_1, the shape of the CV curve shows a pair of redox peaks: one appears around 0.27 V and the other appears around 0.42 V. For the electrode S_2, a pair of redox peaks appears around 0.37 V and 0.5 V. This means that the Faradaic redox reactions have a significant impact on the capacitance of electrode S_1 and S_2. Figure 6b shows the galvanostatic charge–discharge (GCD) curves at the current density of 1 Ag^{-1}. Obviously, it takes a longer time to complete one discharge process (it is ~ 392.4 s for the electrode S_2 and ~ 208.0 s for the electrode S_1), demonstrating that the electrode S_2 shows the larger specific capacitance.

To further investigate the electrochemical behaviors of the electrode S_2 in a three-electrode system, we have done a series of testing under different condition. Figure 7a shows a sequence of CV curves obtained with the potential window ranging from 0 to 0.7 V at various scan rates. With the increase of the voltage sweep rate, the absolute value of the anodic and cathodic peaks increases clearly, revealing a relatively low resistance of the electrode and the fast redox reactions at the interface between the electrode and electrolyte [35]. Figure 7b shows GCD curves of the electrode S_2 obtained at a potential window 0 ~ 0.45 V at different current densities from 1 to 20 Ag^{-1}. The corresponding discharge time is estimated to be 392.4, 193.1, 74.7, 45.8, 36.4, and 17.8 s. According to the above results, the specific capacities of the electrode S_2 and S_1 at different current densities can be calculated by the formula introduced in "Experimental" section and shown in Fig. 7c. The electrode S_1 has a specific capacitance of 458.2, 449.3, 433.6, 416.9, 407.1, and 393.8 Fg^{-1} at a current density of 1, 2, 5, 8, 10, and 20 Ag^{-1}, respectively, while the electrode S_2 has a specific capacitance of 872.0, 858.2, 830.0, 814.2, 808.9, and 791.1 Fg^{-1}. Significantly, compared with the former, the latter (S_2) exhibits the higher capacitance of 872.0 Fg^{-1} at a low current density of 1 Ag^{-1} and retains 791.1 Fg^{-1} even at a high current density of 20 Ag^{-1}. Such an enhanced electrochemical performance for the electrode S_2 should be attributed to its rational material and structure design [36, 37]. In order to check the cycling performance of the electrode S_2, we calculated and presented in Fig. 7d the retention of specific capacitance obtained at current density of 10 Ag^{-1}, finding that the electrode S_2 still retains 92.9% capacitance even after 5000 cycles. The inset shows the last ten GCD curves.

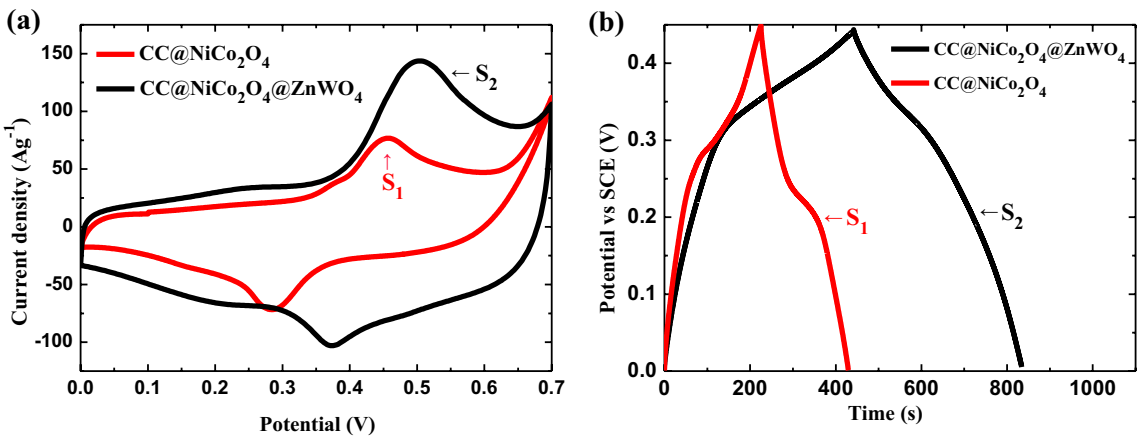

Fig. 6 **a** CV curves of electrode S_1 and S_2 measured at a scan rate of 100 mVs^{-1}, and **b** GCD curves tested at a current density of 1 Ag^{-1} for the electrode S_1 and S_2

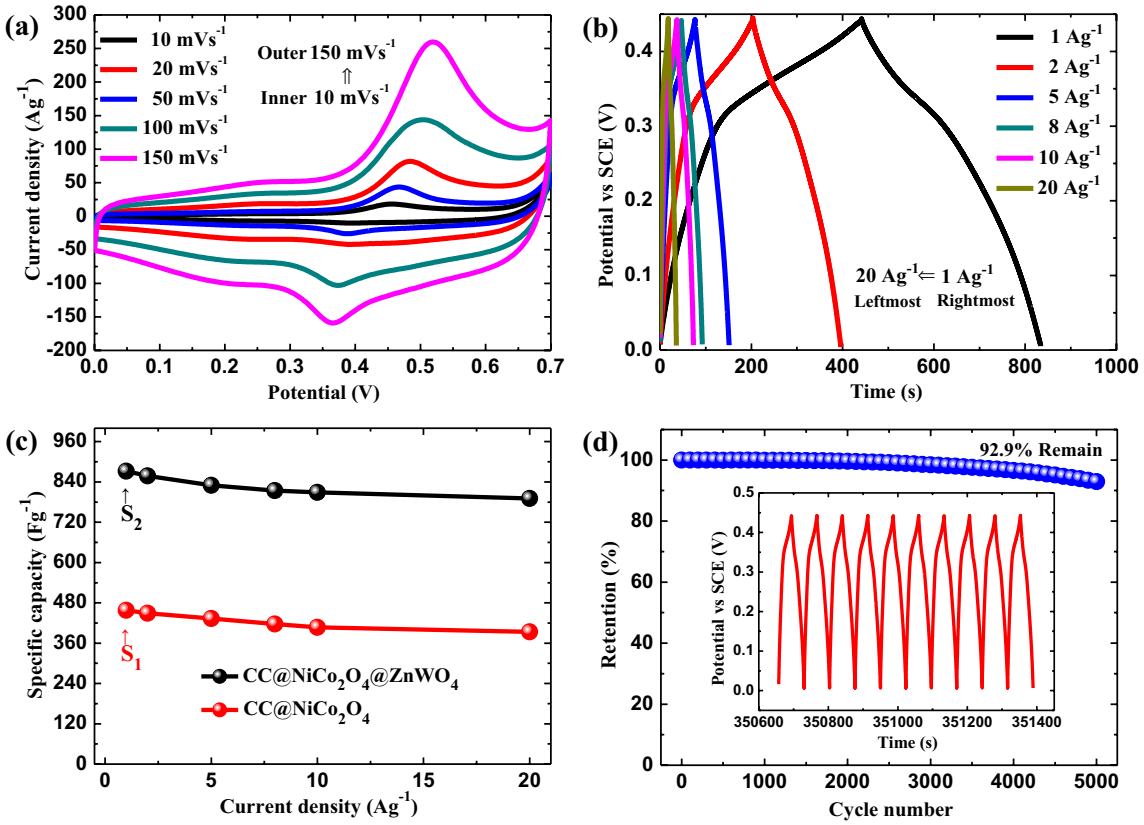

Fig. 7 **a** CV curves measured at different voltage scanning rate and **b** GCD curves obtained at various current densities of the electrode S_2. **c** Specific capacity as a function of current density for the electrode S_1 and S_2. **d** Capacity retention as a function of cycle number for the electrode S_2. The inset shows last ten GCD curves at current density of 10 Ag^{-1}

4 Conclusions

In summary, we have demonstrated the rational design and fabrication of 3D hierarchical $NiCo_2O_4$ nanosheet arrays@$ZnWO_4$ nanoflakes core–shell structures on carbon cloth by a facile and efficient two-step hydrothermal approach following the proper heat treatment. The as-prepared CC@$NiCo_2O_4$ NSAs@$ZnWO_4$ NFs electrode was found to show a high specific capacitance of 872.0 Fg^{-1} at a low current density of 1 Ag^{-1} and still retaining 791.1 Fg^{-1} even at a high current density of 20 Ag^{-1}, revealing its excellent rate capability. After 5000 GCD cycles at the current density of 10 Ag^{-1}, the electrode still kept 92.9% specific capacitance, indicating its great cycling performance. Therefore, the present work provided an insight into the fabrication of novel electrode materials with both enhanced rate capability and cycle performance for potential use in supercapacitors and other energy storage devices.

Acknowledgements This work was supported in part by National Natural Science Foundation of China (Grant Nos. 11332013, 11272364, 11372104, 11372363, 5121543, and 21503025), Chongqing Research Program of Basic Research and Frontier Technology (No. cstc2016jcyjA0366), Students Research Training Program of Chongqing University (No. 2016408).

References

1. W. Wang, W.Y. Liu, Y.X. Zeng, Y. Han, M.H. Yu, X.H. Liu, Y.X. Tong, A novel exfoliation strategy to significantly boost the energy storage capability of commercial carbon cloth. Adv. Mater. **27**, 3572–3578 (2015)
2. Y. Cheng, H. Zhang, C.V. Varanasi, J. Liu, Improving the performance of cobalt-nickel hydroxide-based self-supporting electrodes for supercapacitors using accumulative approaches. Energy Environ. Sci. **6**, 3314–3321 (2013)
3. P. Vialat, C. Mousty, C. Taviot-Gueho, G. Renaudin, H. Martinez, J.C. Dupin, E. Elkaim, F. Leroux, High-performing monometallic cobalt layered double hydroxide supercapacitor with defined local structure. Adv. Funct. Mater. **24**, 4831–4842 (2014)
4. J. Chmiola, C. Largeot, P.L. Taberna, P. Simon, Y. Gogotsi, Monolithic carbide-derived carbon films for micro-supercapacitors. Science **328**, 480–483 (2010)
5. J. Hou, C. Cao, F. Idrees, X. Ma, Hierarchical porous nitrogen-doped carbon sheets derived from silk for ultrahigh capacity battery anodes and supercapacitors. ACS Nano **9**, 2556–2564 (2015)
6. G. Gao, H.B. Wu, S. Ding, L.M. Liu, X.W. Lou, Hierarchical $NiCo_2O_4$ nanosheets grown on Ni nanofoam as high-performance electrodes for supercapacitors. Small **11**, 804–808 (2015)

7. V.H. Nguyen, J.J. Shim, In situ growth of hierarchical mesoporous $NiCo_2S_4$@MnO_2 arrays on nickel foam for high-performance supercapacitors. Electrochim. Acta **166**, 302–309 (2015)
8. X. Tang, R.Y. Jia, T. Zhai, H. Xia, Hierarchical Fe_3O_4@Fe_2O_3 core-shell nanorods arrays as high-performance anodes for asymmetric supercapacitors. ACS Appl. Mater. Interfaces **7**, 27518–27525 (2015)
9. A. Lamberti, A. Gigot, S. Bianco, M. Fontana, M. Castellino, E. Tresso, C.F. Pirri, Self-assembly of graphene aerogel on copper wire for wearable fiber-shaped supercapacitors. Carbon **105**, 649–654 (2016)
10. Z.H. Li, M.F. Shao, L. Zhou, R.K. Zhang, C. Zhang, J.B. Han, M. Wei, D.G. Evans, X. Duan, A flexible all-solid-state micro-supercapacitor based on hierarchical CuO@layered double hydroxide core-shell nanoarrays. Nano Energy **20**, 294–304 (2016)
11. K. Xiao, L.X. Ding, G.X. Liu, H.B. Chen, S.Q. Wang, H.H. Wang, Freestanding hydrophilic nitrogen-doped carbon foam for highly compressible all solid-state supercapacitors. Adv Mater. **28**, 5997–6002 (2016)
12. J. Xu, Z.Q. Tan, W.C. Zeng, G.X. Chen, S.L. Wu, Y. Zhao, K. Ni, Z.C. Tao, M. Ikram, H.X. Ji, Y.W. Zhu, A hierarchical carbon derived from sponge-templated activation of graphene oxide for high-performance supercapacitor electrodes. Adv. Mater. **28**, 5222–5228 (2016)
13. Z.S. Li, X.H. Hu, D.Q. Xiong, B.L. Li, H.Q. Wang, Q.Y. Li, Facile synthesis of bicontinuous microporous/mesoporous carbon foam with ultrahigh specific surface area for supercapacitor application. Electrochim. Acta **219**, 339–349 (2016)
14. U.M. Patil, R.V. Ghorpade, M.S. Nam, A.C. Nalawade, S. Lee, H. Han, S.C. Jun, PolyHIPE derived freestanding 3D carbon foam for cobalt hydroxide nanorods based high performance supercapacitor. Sci. Rep. **6**, 35490–35500 (2016)
15. X.H. Xia, D.L. Chao, Z.X. Fan, C. Guan, X.H. Cao, H. Zhang, H.J. Fan, A new type of porous graphite foams and their integrated composites with oxide/polymer core/shell nanowires for supercapacitors: structural design, fabrication, and full supercapacitor demonstrations. Nano Lett. **14**, 1651–1658 (2014)
16. L.Y. Lin, Q.B. Li, S.Y. Nie, X.H. Peng, N. Hu, 3D $ZnCo_2O_4$ nanowires@MnO_2 nanosheets core-shell structures grown on carbon cloth for excellent supercapacitor electrodes. Ceram. Int. **42**, 19343–19348 (2016)
17. L.F. Chen, Z.Y. Yu, J.J. Wang, Q.X. Li, Z.Q. Tan, Y.W. Zhu, S.H. Yu, Metal-like fluorine-doped β-FeOOH nanorods grown on carbon cloth for scalable high-performance supercapacitors. Nano Energy **11**, 119–128 (2015)
18. Z.H. Pan, Y.C. Qiu, J. Yang, F.M. Ye, Y.J. Xu, X.Y. Zhang, M.N. Liu, Y.G. Zhang, Ultra-endurance flexible all-solid-state asymmetric supercapacitors based on three-dimensionally coated MnO_x nanosheets on nanoporous current collectors. Nano Energy **26**, 610–619 (2016)
19. Z.Y. Yu, L.F. Chen, S.H. Yu, Growth of $NiFe_2O_4$ nanoparticles on carbon cloth for high performance flexible supercapacitors. J. Mater. Chem. A **2**, 10889–10894 (2014)
20. L.Y. Lin, J.L. Liu, T.M. Liu, J.H. Hao, K.M. Ji, R. Sun, W. Zeng, Z.C. Wang, Growth-controlled $NiCo_2S_4$ nanosheet arrays with self-decorated nanoneedles for high-performance pseudocapacitors. J. Mater. Chem. A **3**, 17652–17658 (2015)
21. S.J. Song, F.W. Ma, G. Wu, D. Ma, W.D. Geng, J.F. Wan, Facile self-templating large scale preparation of biomass-derived 3D hierarchical porous carbon for advanced supercapacitors. J. Mater. Chem. A **3**, 18152–18162 (2015)
22. S. Hussain, P.P. Wan, N. Aslam, G.J. Qiao, G.W. Liu, Ag-doped NiO porous network structure on Ni foam as electrode for supercapacitors. J. Mater. Sci. Mater. Electron. **29**, 1759–1765 (2018)
23. L.Y. Lin, T.M. Liu, J.L. Liu, R. Sun, J.H. Hao, K.M. Ji, Z.C. Wang, Facile synthesis of groove-like $NiMoO_4$ hollow nanorods for high-performance supercapacitors. Appl. Surf. Sci. **360**, 234 – 239 (2016)
24. H.Y. Mi, X.G. Zhang, X.G. Ye, S.D. Yang, Preparation and enhanced capacitance of core-shell polypyrrole/polyaniline composite electrode for supercapacitors. J. Power Sources **176**, 403–409 (2008)
25. D.B. Yu, B. Wu, L. Ge, L. Wu, H.T. Wang, T.W. Xu, Decorating nanoporous ZIF-67-derived $NiCo_2O_4$ shells on a Co_3O_4 nanowire array core for battery-type electrodes with enhanced energy storage performance. J. Mater. Chem. A **4**, 10878–10884 (2016)
26. T.F. Qiu, B. Luo, M. Giersig, E.M. Akinoglu, L. Hao, X.J. Wang, L. Shi, M.H. Jin, L.J. Zhi, Au@MnO_2 core-shell nanomesh electrodes for transparent flexible supercapacitors. Small **10**, 4136–4141 (2014)
27. B.K. Guan, L.L. Hu, G.H. Zhang, D. Guo, T. Fu, J.D. Li, H.G. Duan, C.C. Li, Q.H. Li, Facile synthesis of $ZnWO_4$ nanowall arrays on Ni foam for high performance supercapacitors. RSC Adv. **4**, 4212–4217 (2014)
28. X.J. Liu, J.F. Liu, X.M. Sun, $NiCo_2O_4$@NiO hybrid arrays with improved electrochemical performance for pseudocapacitors. J. Mater. Chem. A **3**, 13900–23905 (2015)
29. D.Z. Kong, W.N. Ren, C.W. Cheng, Y. Wang, Z.X. Huang, H.Y. Yang, Three-dimensional $NiCo_2O_4$@Polypyrrole coaxial nanowire arrays on carbon textiles for high-performance flexible asymmetric solid-state supercapacitor. ACS Appl. Mater. Interfaces **7**, 21334–21346 (2015)
30. F.Z. Deng, J.J. Tie, B. Lan, M. Sun, S.M. Peng, S.H. Deng, B.Y. Li, W.J. Sun, L. Yu, $NiCo_2O_4$/MnO_2 heterostructured nanosheet: influence of preparation conditions on its electrochemical properties. Electrochim. Acta **176**, 259–268 (2015)
31. C.Y. Cui, J.T. Xu, L. Wang, D. Guo, M.L. Mao, J.M. Ma, T.H. Wang, Growth of $NiCo_2O_4$@$MnMoO_4$ nanocolumn arrays with superior pseudocapacitor properties. ACS Appl. Mater. Interfaces **8**, 8568–8575 (2016)
32. G. Li, W.Y. Li, K.B. Xu, R.J. Zou, Z.G. Chen, J.Q. Hu, Sponge-like $NiCo_2O_4$/MnO_2 ultrathin nanoflakes for supercapacitor with high-rate performance and ultra-long cycle life. J. Mater. Chem. A **2**, 7738–7741 (2014)
33. J. Liang, Z.Y. Fan, S. Chen, S.J. Ding, G. Yang, Hierarchical $NiCo_2O_4$ nanosheets@halloysite nanotubes with ultrahigh capacitance and long cycle stability as electrochemical pseudocapacitor materials. Chem. Mater. **26**, 4354–4360 (2014)
34. R.B. Rakhi, W. Chen, D. Cha, H.N. Alshareef, Substrate dependent self-organization of mesoporous cobalt oxide nanowires with remarkable pseudocapacitance. Nano Lett. **12**, 2559 – 2567 (2012)
35. G.P. Wang, L. Zhang, J.J. Zhang, A review of electrode materials for electrochemical supercapacitors. Chem. Soc. Rev. **41**, 797 – 828 (2012)
36. R. Ang, Z.C. Wang, C.L. Chen, J. Tang, N. Liu, Y. Liu, W.J. Lu, Y.P. Sun, T. Mori, Y. Ikuhara, Atomistic origin of an ordered superstructure induced superconductivity in layered chalcogenides. Nat. commun. **6**, 6091 (2015)
37. Z.C. Wang, M. Saito, K.P. McKenna, L. Gu, S. Tsukimoto, A.L. Shluger, Y. Ikuhara, Atom-resolved imaging of ordered defect superstructures at individual grain boundaries. Nature **479**, 380–383 (2011)